

RESEARCH ARTICLE | AUGUST 08 2023

Toward using the Villari effect for non-destructive evaluation of steel structures

C. A. Ives   ; S. G. H. Staples  ; C. K. Vo  ; D. M. J. Cowell  ; S. Freear  ; B. T. H. Varcoe 

 Check for updates

J. Appl. Phys. 134, 065101 (2023)

<https://doi.org/10.1063/5.0147736>



CrossMark

Articles You May Be Interested In

Output characteristics and experimental study of a highly linear and large-range force sensor based on the Villari effect

AIP Advances (May 2021)

Model for the effect of tensile and compressive stress on ferromagnetic hysteresis

Journal of Applied Physics (April 1987)

Progress in development of Jiles-Atherton model of magnetic hysteresis

AIP Conference Proceedings (July 2019)



Instruments for Advanced Science

- Knowledge
- Experience
- Expertise

Click to view our product catalogue

Contact Hiden Analytical for further details:

www.HidenAnalytical.com

info@hiden.co.uk

Gas Analysis



- ▶ dynamic measurement of reaction gas streams
- ▶ catalysis and thermal analysis
- ▶ molecular beam studies
- ▶ dissolved species probes
- ▶ fermentation, environmental and ecological studies

Surface Science



- ▶ UHV-TPD
- ▶ SIMS
- ▶ end point detection in ion beam etch
- ▶ elemental imaging - surface mapping

Plasma Diagnostics



- ▶ plasma source characterization
- ▶ etch and deposition process reaction kinetic studies
- ▶ analysis of neutral and radical species

Vacuum Analysis



- ▶ partial pressure measurement and control of process gases
- ▶ reactive sputter process control
- ▶ vacuum diagnostics
- ▶ vacuum coating process monitoring

Toward using the Villari effect for non-destructive evaluation of steel structures

Cite as: J. Appl. Phys. 134, 065101 (2023); doi: 10.1063/5.0147736

Submitted: 25 February 2023 · Accepted: 18 July 2023 ·

Published Online: 8 August 2023



View Online



Export Citation



CrossMark

C. A. Ives,^{1,a)}  S. G. H. Staples,¹  C. K. Vo,²  D. M. J. Cowell,²  S. Freear,²  and B. T. H. Varcoe¹ 

AFFILIATIONS

¹Quantum Experimental Group, School of Physics and Astronomy, University of Leeds, LEEDS, West Yorkshire LS2 9JT, United Kingdom

²School of Electronic and Electrical Engineering, University of Leeds, LEEDS, West Yorkshire LS2 9JT, United Kingdom

^{a)}Author to whom correspondence should be addressed: ives.carol.a@gmail.com

ABSTRACT

This work follows on from studies carried out by Jiles and Atherton on magnetic hysteresis and on the magnetomechanical effect. The Jiles–Atherton equation, which models the rate of change of magnetization with respect to stress, was solved numerically in the forward and reverse directions for stress up to 90 MPa, suggesting that stressing carbon steel will cause a lasting change in the magnetization of the sample. This was confirmed experimentally by measuring the **B**-field in proximity to samples of C45 steel while undergoing tensile stress, with the pattern of magnetization suggesting that the magnetic domains reorient themselves in the geomagnetic field when stressing loosens their pinning. A further experiment on two samples confirms this, with the **B**-field around the samples showing strong changes according to their orientation in the geomagnetic field at the time of the stressing. This work has relevance to the non-destructive testing of steel structures such as pipelines, and the relevance of the experiments to this work is considered, as well as future prospects.

Published under an exclusive license by AIP Publishing. <https://doi.org/10.1063/5.0147736>

I. INTRODUCTION

Steel is widely used for extensive structures such as pipelines, bridges, and towers, and these require methods of non-destructive evaluation (NDE) to ensure their efficiency and safety. NDE allows steel to be checked for faults and stresses without disturbing the structure itself. As steel is ferromagnetic, it is potentially well suited to magnetic methods of NDE. Some of these magnetic methods of NDE utilize the Villari effect,¹ whereby the deformation of a sample of metals, or an applied stress, alters the magnetic field around the sample.

The Villari effect is the inverse of the Joule effect,² or magnetostriction, whereby the dimensions of a ferromagnetic sample change when subjected to a magnetic field, this being due to the magnetic domains of the metal aligning themselves in the direction of the applied field, through a process of both domain wall motion and domain rotation. Conversely, the Villari effect is due to stress causing a change in the shape of the magnetic domains through a shift in the domain walls, and these changes then alter the surrounding magnetic field due to the sample. A good overview of these magnetomechanical effects was given by Lee.³ The Villari

effect, in particular, is pertinent to the NDE of steel structures, allowing for measurements of the magnetic field around a steel section to give an indication of whether the material is stressed, and potentially to reveal stress concentration zones. If the magnetic field created due to the Villari effect in carbon steel can be characterized by experiments, modeling different types of stress may allow the characterization of the different defect signatures allowing the prediction of problem areas in steel structures. To this end, Staples *et al.*⁴ looked at the inverse problem of determining the stress undergone by a sample of steel by observing its surrounding **B**-field, in order to model this relationship for use in the NDE of steel structures. They found a high level of correspondence between theoretical calculations using multi-physics modeling tool COMSOL and experimental observations, and concluded that the magnetic field resulting from a steel bar being subjected to a stress cycle suggests that magnetic poles are formed at either end of the stress concentration zone. Additionally, Staples *et al.*⁵ modeled the pipeline as a series of magnetic dipoles, allowing the analysis of magnetic flux leakage using a large stand off magnetometry technique. Their experimental work in the field showed this technique to be viable for the NDE of underground pipelines, determining

07 September 2023 08:22:43

the location of stress concentration zones, such as welds, with a probability of detection of 88% at ± 2 m.

II. THEORETICAL WORK

Based on their theory of ferromagnetic hysteresis,⁶ a model of the relationship between stress and magnetization has been provided by Jiles and Atherton⁷ and developed into a theory of the magnetomechanical effect.⁸

Ferromagnetic hysteresis arises due to a frictional force which opposes changes in magnetization. This idea was first proposed by Wiedemann,⁹ and Jiles and Atherton⁶ included it in their theory of ferromagnetic hysteresis. They proposed that this opposing frictional force is due to a pinning of domain walls by defect sites inside the solid, utilizing a model of domain wall motion provided by Globus and Duplex.^{10,11} Jiles and Atherton⁶ adapted this model of domain wall pinning quantitatively by assuming a mean pinning energy per site and that pinning sites are distributed uniformly throughout the solid.

It is the Jiles–Atherton model of ferromagnetic hysteresis that has directly addressed the relationship between magnetization and stress, with Jiles⁸ building on this to form a theory of the magneto-mechanical, or Villari, effect. Previously, Craik and Wood¹² had conducted extensive experimental work on the Villari effect with a variety of specimens, and Birss, Faunce, and Isaac¹³ had found that the dependence of magnetization on stress was asymmetric with respect to tension and compression. Jiles⁸ looked at the changes in magnetization a ferromagnetic material undergoes when subjected to applied uniaxial stress, and also sought to explain the existing experimental results, particularly to find an adequate explanation for the form of the curves found by previous groups.^{12,13} Jiles⁸ proposed that the main mechanism of the Villari effect is that domain walls tend to be pinned on defect sites within the lattice, and an applied stress causes some of the domain walls to break away from these pinning sites, moving toward anhysteretic equilibrium until the domain walls encounter further defect sites and are pinned again. This process leads to irreversible changes in the magnetization with field and so to hysteresis in the magnetization. The changes in magnetization are explained by both this domain wall

motion and rotation of magnetization, and in the low field region, such as the geomagnetic field, domain wall motion is the dominant mechanism, (Jiles and Atherton⁷), hence the significance of the pinning sites in the low field region. It was also proposed that this change in magnetization reduces the displacement from the anhysteretic magnetization, and additionally, the anhysteretic magnetization itself is changed by the application of stress via magnetoelastic coupling. The key ideas of this model theory were encapsulated in the Jiles⁸ equation [Eq. (1)] in which the rate of change of magnetization with stress, $\frac{dM}{d\sigma}$, is proportional to the displacement of the irreversible magnetization, M_{irr} , from the anhysteretic magnetization, dM_{an} . This proportionality of rate of change to the displacement was called the “law of approach,” which seems to apply when the starting condition of the material is on a major hysteresis loop,

$$\frac{dM}{d\sigma} = \frac{1}{E\xi} \sigma(1 - c)(M_{an} - M_{irr}) + c \frac{dM_{an}}{d\sigma}. \quad (1)$$

The irreversible magnetization, M_{irr} , is magnetization achieved when all the domain walls are returned to their planar condition and all reversible rotations of domain magnetizations are relaxed back to zero. c represents the flexibility of the magnetic domain walls, E is the Young modulus, and ξ is the model coefficient.

It initially appears that, in principle, solving the Jiles–Atherton equation would allow the plotting of a theoretical curve for magnetization M as a function of stress σ . However, the Jiles–Atherton equation cannot be solved analytically.

Rewriting the Jiles–Atherton equation in terms of its component variables, listed in Table I, gives

$$\frac{dM}{d\sigma} = \frac{\frac{\sigma}{\xi^2} \left(M_s \left[\coth\left(\frac{H+H_\sigma+\alpha M}{a}\right) - \frac{a}{H+H_\sigma+\alpha M} \right] - M \right)}{\left(1 - cM_s \left(\frac{\alpha a}{(H+H_\sigma+\alpha M)^2} - \frac{\alpha \operatorname{csch}^2\left(\frac{H+H_\sigma+\alpha M}{a}\right)}{a} \right) \right)}, \quad (2)$$

which allows $\frac{dM}{d\sigma}$ to be expressed in terms of σ , M , and $H_\sigma(\sigma, M)$.

Equation (2) was solved numerically, using the Matlab function ode45, an ordinary differential equation (ODE) solver that

TABLE I. Values used for variables when plotting the Jiles–Atherton equation using Matlab: the values are taken from Jiles,⁸ H is the equivalent of the geomagnetic field, and T is taken to be 300 K.

Variable	Symbol	Value	Units
Young modulus	E	210×10^9	Pa
Model coefficient	ξ	605	J m^{-3}
Saturation magnetization	M_s	1.71×10^6	A m^{-1}
Applied magnetic field (geomagnetic field)	H	37	A m^{-1}
Strength of coupling of individual magnetic moments	α	0.0011	...
Temperature	T	300	K
Flexibility of magnetic domain walls	c	0.1	...
Curve fit coefficient	$\gamma_1(0)$	7×10^{-18}	$\text{A}^{-2} \text{m}^2$
Curve fit coefficient	$\gamma'_1(0)$	-1×10^{-25}	$\text{A}^{-2} \text{m}^2 \text{Pa}^{-1}$
Curve fit coefficient	$\gamma_2(0)$	-3.3×10^{-30}	$\text{A}^{-4} \text{m}^2$
Curve fit coefficient	$\gamma'_2(0)$	2.1×10^{-38}	$\text{A}^{-4} \text{m}^4 \text{Pa}^{-1}$

07 September 2023 08:22:43

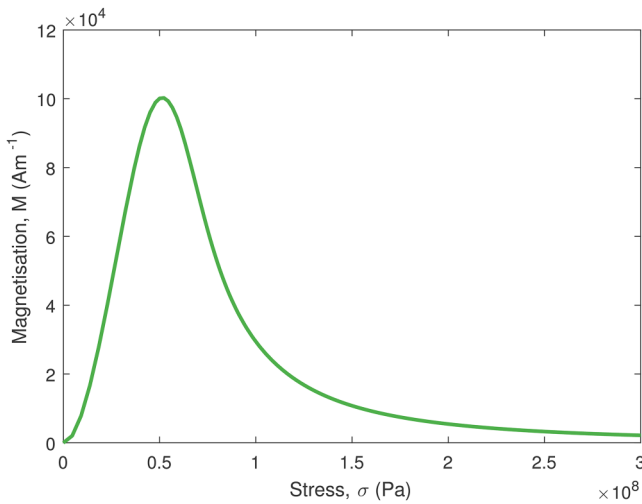


FIG. 1. Equation (2) was solved numerically for the forward curve, using the Matlab function ode45, producing this plot of magnetization, M , vs stress, σ .

utilizes fourth- and fifth-order Runge–Kutta methods. The parameter values used were those given in Jiles⁸ and given in Table I. This solution allowed a plot of magnetization M as a function of stress σ , from 0 to 300 MPa, as shown in Fig. 1. Attempting to solve the equation in the reverse direction, from 300 MPa back to zero stress, found that M tends to infinity as stress tends to zero, as shown in Fig. 2. If a lower maximum stress is plotted of around 90 MPa, as shown in Fig. 3, then a curve similar to that of Li and Jiles¹⁴ is found, leading to the

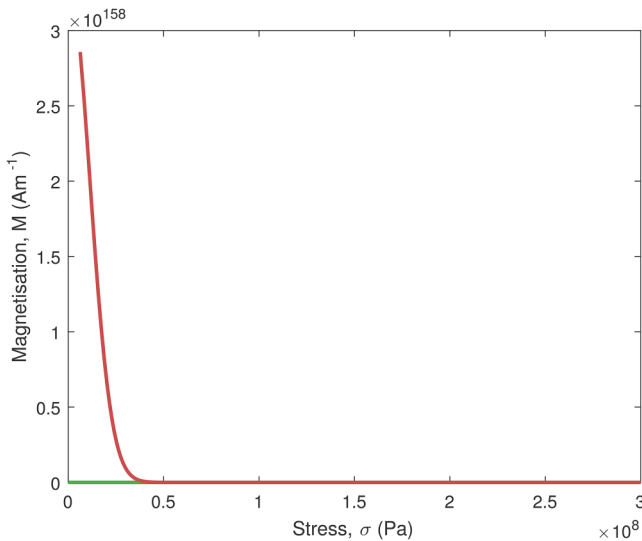


FIG. 2. Equation (2) was solved numerically for the forward curve (green) and the reverse curve (red), using the Matlab function ode45, producing this plot of magnetization, M , vs stress, σ , up to a stress level of 300 MPa.

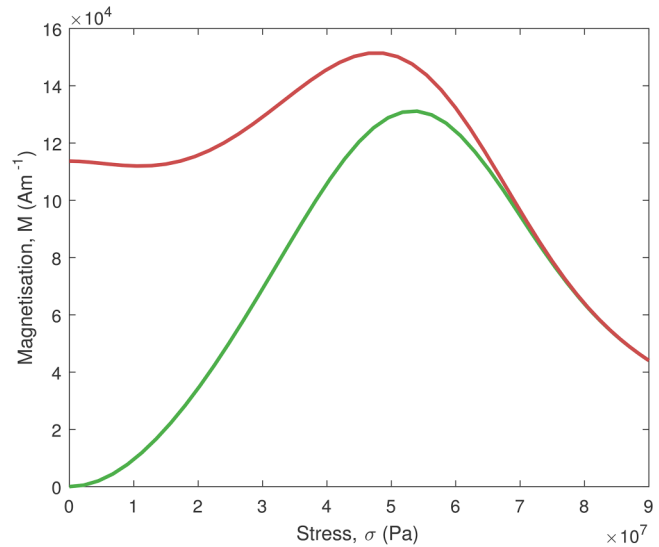


FIG. 3. Equation (2) was solved numerically for the forward curve (green) and the reverse curve (red), using the Matlab function ode45, producing this plot of magnetization, M , vs stress, σ , up to a stress level of 90 MPa.

conclusion that the model is very sensitive to maximum stress level used. The forward curves show a maximum value of M at around 10^5 A m^{-1} , which seems like a surprisingly high magnetic field strength to be found when stressing a steel sample. It is noticeable also that this maximum value of magnetization occurs at around 60 MPa, which seems like a relatively low level of stress to produce such a large change in magnetization. Thus, it was not found to be straightforward to reproduce the curve from the Jiles–Atherton equation as solved and plotted by Li and Jiles¹⁴ at the higher stress levels, and the curves produced for the lower stress levels, such as 90 MPa, can only be regarded as an approximation to a solution.

The calculated variation of magnetization with stress given by Li and Jiles¹⁴ suggests that under tension the magnetization of steel due to the stress increases to a maximum, and that when the tension is released the magnetization of the steel falls, but not to its original level. This is such that when stress is relaxed back down to zero, a certain degree of magnetization of the sample due to the stress remains. A similar effect was found experimentally for mild steel by Craik and Wood,¹² where it was found that magnetization due to stress increased with stress, and then this elevated level of magnetization remained upon relaxation. Similar results for mild steel were also found by Birss, Faunce, and Isaac.¹³ One of the objectives of the experimental work in this study was to see if this effect was found.

TABLE II. The composition of C45 carbon steel.¹⁵

	C	Si	Mn	Cr	Ni	Others
Weight %	0.42–0.50	0.17–0.37	0.50–0.80	<0.25	<0.25	0.035

07 September 2023 08:22:43

TABLE III. The properties of C45 carbon steel.¹⁵

Elastic (Young, tensile) modulus	Tensile yield strength
210 GPa	340–570 MPa

III. EXPERIMENT 1: MEASURING THE B-FIELD IN PROXIMITY TO STEEL BARS UNDERGOING SUCCESSIVE CYCLES OF TENSILE STRESS AND RELAXATION

A. Experiment 1: Motivation

Extended steel structures, such as pipelines and bridges, are particularly subject to tension. This tension can be cyclical in nature, such as according to temperature changes over days and seasons, and also according to cyclical pressure changes in the way the structure is used. With pipelines, such cyclical pressure changes can be due to changes and surges in the supply of oil and gas. Hence, the first set of experiments looked at changes in the magnetic field around samples of steel placed under three successive cycles of tension followed by relaxation.

On the basis of the solution to the Jiles–Atherton equation [Eq. (1)] plotted by Li and Jiles,¹⁴ and the previous experimental results,^{12,13} it was hypothesized that subjecting the steel samples to tensile stress on the first cycle would cause the level of magnetization M of the samples to increase with increasing stress, and that, despite decreasing the stress level to zero, the magnetization M of the steel samples would not fall to the original level, but would remain elevated. Additionally, it was expected that although on the second and third cycles the magnetization might increase further, that this would not be to the same extent as on the first cycle.

The magnetization of the steel sample would be inferred from the measurement of the \mathbf{B} -field in close proximity to the sample, according to $\mathbf{B} = \mu_0(\mathbf{H} + \mathbf{M})$.

B. Experiment 1: Three-cycle tests of tension and relaxation of steel samples

A set of three-cycle tests were carried out on five previously untested steel samples of C45 medium carbon steel of approximately 3.0 mm in thickness, with widths varying from 4.0 to 20.0 mm. The steel composition and properties are given in Tables II and III.¹⁵ Prior to the experiment, the samples were prepared by a degaussing technique, to reduce their level of magnetization. The stress range that was looked at in this set of tests was that prior to plastic

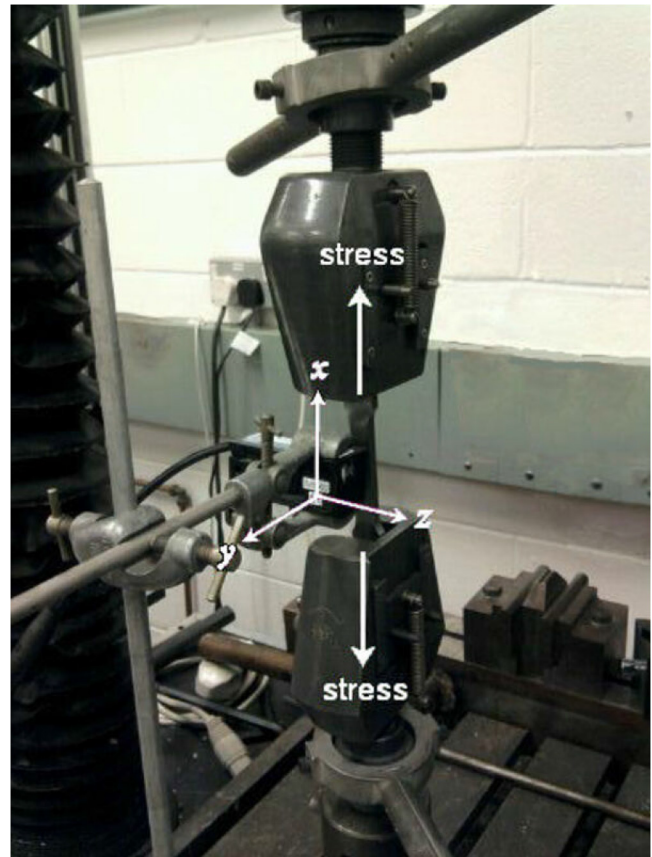


FIG. 4. Experiment 1: experimental setup with steel dumbbell held in the jaws of the tensile stress machine, and the magnetometer in place. Magnetometer axes are shown and direction of stress.

07 September 2023 08:22:43

deformation, because the Jiles–Atherton equation is derived from equations for the rate of change of magnetization M with respect to elastic energy W , resulting from applied stress. The test sample measurements and shapes, distance of magnetometer from sample, maximum force, and maximum stress are shown in Table IV.

A servo mechanical tensile test machine (RDP Howden) was used to place the samples under tensile stress, (Fig. 4), with the

TABLE IV. Experiment 1: Three-cycle tests of stress and relaxation of steel bars. The C45 steel samples varied in width as shown and were all of approximately 3.0 mm thickness.

Test No.	1	2	3	4	5
Approx width of middle section of sample (mm)	4.0	6.0	8.0	12.0	20.0
Approx sample length (mm)	200	200	200	200	211
Sample shape	Dumbbell	Dumbbell	Dumbbell	Dumbbell	Straight
Magnetometer distance from sample (cm)	9.5	14.5	7.0	7.0	7.0
Maximum force (kN)	5.01	5.11	6.74	11.17	10.12
Maximum stress (MPa)	407.09	281.32	280.73	306.72	167.15

TABLE V. Experiment 1: B-field vectors for background, published data for Leeds,¹⁶ B-field vector for machine in both stressing and relaxing operation. Values for \mathbf{B}_{local} , **Machine field, stressing** and **Machine field, relaxation** all have an error of $\leq \pm 60$ nT.

		i, (nT)	j, (nT)	k, (nT)	Magnitude, (nT)
Published data for geomagnetic field at Leeds, (53.80 N, 1.55 W)		-45, 737 ± 18	49, 243 ± 21
\mathbf{B}_{local}	Test 1	-41, 536	-17, 177	-3, 703	45, 100
	Test 2	-41, 281	-9, 149	-6, 889	42, 840
	Test 3	-41, 437	-27, 190	-12, 132	51, 024
	Test 4	-41, 102	-29, 246	-12, 553	51, 983
	Test 5	-30, 500	-29, 148	-14, 066	44, 472
Machine field, stressing, $\mathbf{B}_{machine1}$	Test 1	3, 400	1, 460	-380	3, 730
	Test 2	2, 900	1, 370	-320	3, 220
	Test 3	4, 290	1, 980	-190	4, 720
	Test 4	4, 690	2, 080	-240	5, 130
	Test 5	3, 930	1, 900	-45	4, 360
Machine field, relaxation, $\mathbf{B}_{machine2}$	Test 1	2, 900	1, 170	-370	3, 200
	Test 2	2, 560	1, 040	-400	2, 790
	Test 3	3, 900	1, 700	-180	4, 300
	Test 4	4, 400	1, 850	-270	4, 800
	Test 5	3, 500	1, 690	-140	3, 880

force on the sample, and the \mathbf{B} -field in the x -, y - and z -directions at a fixed point from the sample, being measured.

Each steel sample was stretched up to the maximum force as given in Table IV, a force calculated to keep the sample within the elastic limit of deformation. After approximately 20 s at maximum force, the sample was then relaxed back down to zero force, and after approximately 20 s the cycle was repeated, each sample undergoing three such cycles in total.

C. Experiment 1: Results

Prior to conducting each of the five tests, a reading was taken of the local magnetic field, \mathbf{B}_{local} . For each experiment, \mathbf{B}_{local} was subtracted from the overall \mathbf{B} -field measurement along with values of the \mathbf{B} -field attributable to the tensile test machine in operation. The \mathbf{B} -field value attributable to the machine was found to be slightly different for stressing, $\mathbf{B}_{machine1}$, and relaxing, $\mathbf{B}_{machine2}$, conditions, with stressing producing a slightly greater magnitude of \mathbf{B} -field. Both $\mathbf{B}_{machine1}$ and $\mathbf{B}_{machine2}$ were found to be marginal in comparison with the geomagnetic field,¹⁶ being less than 10% of the magnitude of \mathbf{B}_{local} . \mathbf{B}_{local} and the \mathbf{B} -field of the machine in operation ($\mathbf{B}_{machine1}$ on stressing, and $\mathbf{B}_{machine2}$ on relaxation) were subtracted from the overall \mathbf{B} -field measurement, to give the difference in \mathbf{B} , $\Delta\mathbf{B}$, attributable to the stressing of the sample. Values for \mathbf{B}_{local} , along with $\mathbf{B}_{machine1}$ and $\mathbf{B}_{machine2}$ values are shown in Table V.

On the first cycle, for all five tests, the magnitude of $\Delta\mathbf{B}$ increased with increasing stress, and remained at this elevated level as the stress was reduced back to zero, as shown in Fig. 5. For the second and third cycles, the magnitude of $\Delta\mathbf{B}$ at maximum stress increased successively, but not to the extent of the first cycle. These results are consistent with the curve produced by Li and Jiles¹⁴ which suggests that uniaxial tension and subsequent relaxation of a steel bar will produce the hysteretic effect of the stress-

magnetization curve being higher on the return journey, as the stress is reduced, compared with the outward journey as the stress is increasing. Thus, we would expect this pattern to be reflected in the behavior of the \mathbf{B} -field at the point of the magnetometer.

Additionally, when this effect was compared for the varying widths of steel sample, by plotting $|\Delta\mathbf{B}|$ at 150MPa on the first cycle vs cross-sectional area of sample, as shown in Fig. 6, it was found that $|\Delta\mathbf{B}|$ clearly increased as a positive function of the sample cross section, indicating that $|\Delta\mathbf{B}|$ is greater where the bulk of the sample is larger for identical stress levels. This provides clear confirmation that the change in magnetization with stress is greater where there is a greater bulk of the sample and is thus related to bulk magnetization. Figure 7 shows all five first cycles on the same plot, indicating that greater levels of stress were achieved for the thinner samples, and that the gradient of the outward stress-magnetization curve increased as a positive function of sample width, again, attributable to the greater change in $|\Delta\mathbf{B}|$ as a positive function of the bulk of the sample. Similarly, Staples *et al.* 2013⁴ found a direct correlation between the sample width and the overall intensity of remanent magnetization.

For the x -, y -, and z -components of $\Delta\mathbf{B}$ (Figs. 8–10), there were distinctive and similar patterns across all five tests. For all tests, with the exception of test 5, it was ΔB_x that reached the highest values and thus formed the greater part of $\Delta\mathbf{B}$ at all stress levels, reaching values in the approximate range of 2500–8000 nT. This is to be compared with values from -600 to 1,400 nT and -225–40 nT for ΔB_y and ΔB_z , respectively. Anomalously, for test 5, the greater contribution to the magnitude of $\Delta\mathbf{B}$ came from ΔB_y , which reached values of around 4000 nT, whereas ΔB_x for this test only reached values of 1500 nT. For test 5, the shape of the ΔB_y curve most closely resembled that of the curve for magnitude of $\Delta\mathbf{B}$. Since the x axis is parallel with the length of the bar, it is to be expected that ΔB_x would show the highest value, since there is more bulk of steel in this

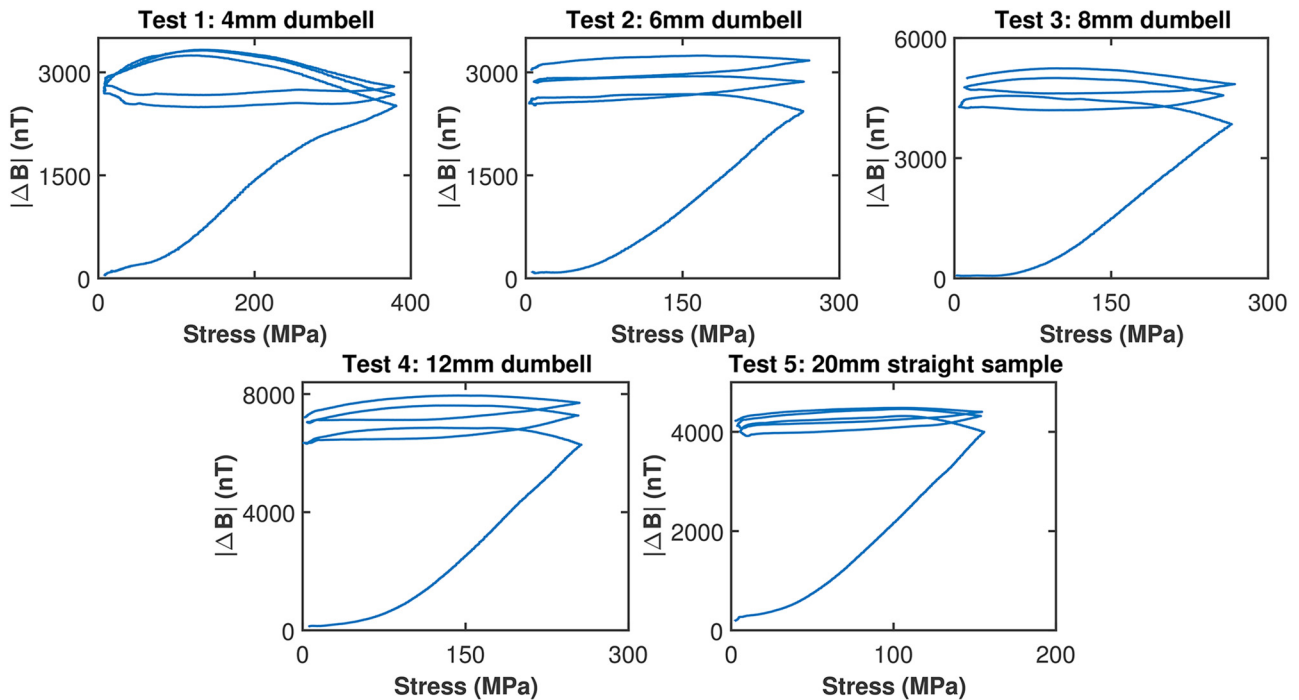


FIG. 5. Experiment 1: Magnitude of ΔB as a function of stress σ for all five samples, with stressing starting at the origin (0,0). The plots show that the magnitude of the B -field increases upon first cycle stressing and remains at an elevated level upon relaxation, with the subsequent two cycles only leading to a marginal increase in $|\Delta B|$. This is the same pattern across all five tests.

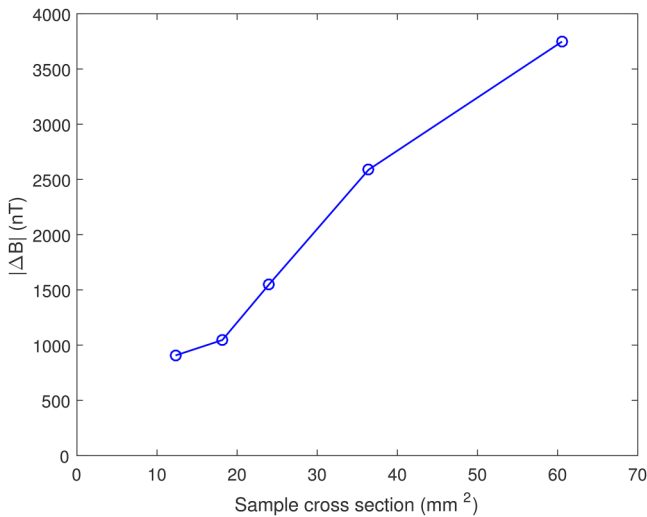


FIG. 6. Experiment 1: $|\Delta B|$ at 150 MPa stress on first cycle vs cross-sectional area of sample. The positive relationship indicates that the greater the bulk of the steel, the greater the change in the magnetic field for the same level of stress.

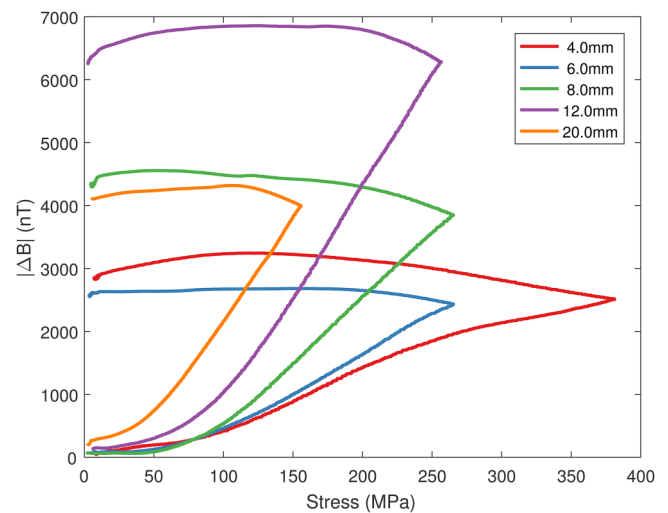


FIG. 7. Experiment 1: The first stress cycle for each of the five samples, plotting $|\Delta B|$ vs stress and starting at the origin (Savitzky-Golay filter applied to B -field data). $|\Delta B|$ increases with increasing stress, and then remains at the elevated level upon relaxation.

07 September 2023 08:22:43

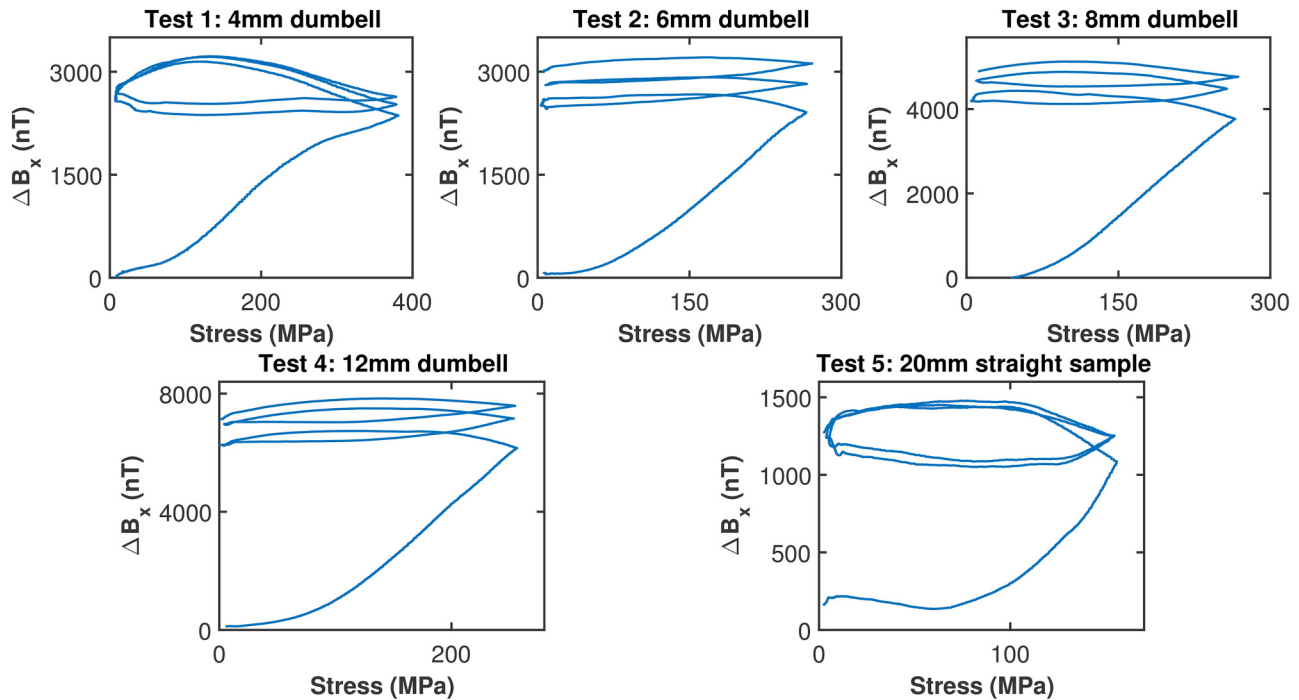


FIG. 8. Experiment 1: x -component of $\Delta\mathbf{B}$ as a function of stress σ for all five samples, with stressing starting at the origin (0,0).

direction. Additionally, the negative x -direction is also approximately the direction of the Earth’s magnetic field and, if the domains are lining up in the direction of the Earth’s field, this direction would show the most changes. As for test 5, it is possible that the change in magnetization was more pronounced in the y -direction due to stray fields, or the possibility that the straight samples are not directly comparable with the dumbbells. ΔB_y generally showed a shift in the positive direction except for test 2, where it went negative. For tests 1–4, ΔB_z was negative, but for test 5, it was positive.

The change in $\Delta\mathbf{B}$ as measured by the magnetometer was predominantly in the positive x -direction which is in the opposite direction to the geomagnetic field which is pointing approximately in the negative x -direction. Considering the \mathbf{B} -field around a bar magnet, as shown in Fig. 11, we see that the direction of the \mathbf{B} -field outside, but in proximity to, the bar magnet is pointing in the opposite direction to the \mathbf{B} -field within the bar. This suggests that stressing a steel bar causes its \mathbf{B} -field to start to line up with that of the local \mathbf{B} -field, which is predominantly the geomagnetic field, which is what might be expected. This idea is supported when we look at the dot products for the unit vectors of the background field vector for each test and the final vector for $\Delta\mathbf{B}$ at the end of the stress cycling as shown in Table VI, showing strong negative correlation in the directions of these two vectors for each of the five tests.

D. Experiment 1: Discussion

The results of the three-cycle tests show clearly that the stressing of the samples leads to a shift in the \mathbf{B} -field around the sample,

which remains after the stressing has ended, suggesting a lasting shift in the bulk magnetization of the sample. There is an increase in $\Delta\mathbf{B}$ in the positive x -direction for all five tests, with this being the predominant shift in the \mathbf{B} -field, with varied results for the y - and z -directions. The results support the experimental hypothesis that there would be an increase in the magnitude of $\Delta\mathbf{B}$ that would remain after stressing. The fact that the change is predominantly in the positive x -direction suggests that the domains are lining up in the geomagnetic field which lies predominantly in the negative x -direction, causing an increase in the \mathbf{B} -field in the opposite direction at the point of the magnetometer which lies in the external \mathbf{B} -field of the sample, as shown in Fig. 11. If stressing unpins the magnetic domains allowing them to move, it would be reasonable to assume that the magnetic moment of each newly unpinned domain would line up in the Earth’s magnetic field due to the torque exerted on it, according to

$$\boldsymbol{\tau} = \boldsymbol{\mu} \times \mathbf{B} \tag{3}$$

and thus reducing its potential energy.

Looking at the successive cycles of stress and relaxation: although the initial stress cycle caused a clear and lasting change in the sample, the subsequent two cycles caused a more marginal change in the same direction. This may be due to the system being close to saturation whereby the limit for unpinning of the domains has been reached in this situation and $\Delta\mathbf{B}$ will not change any further. In terms of the Jiles–Atherton theory, it could be said that

07 September 2023 08:22:43

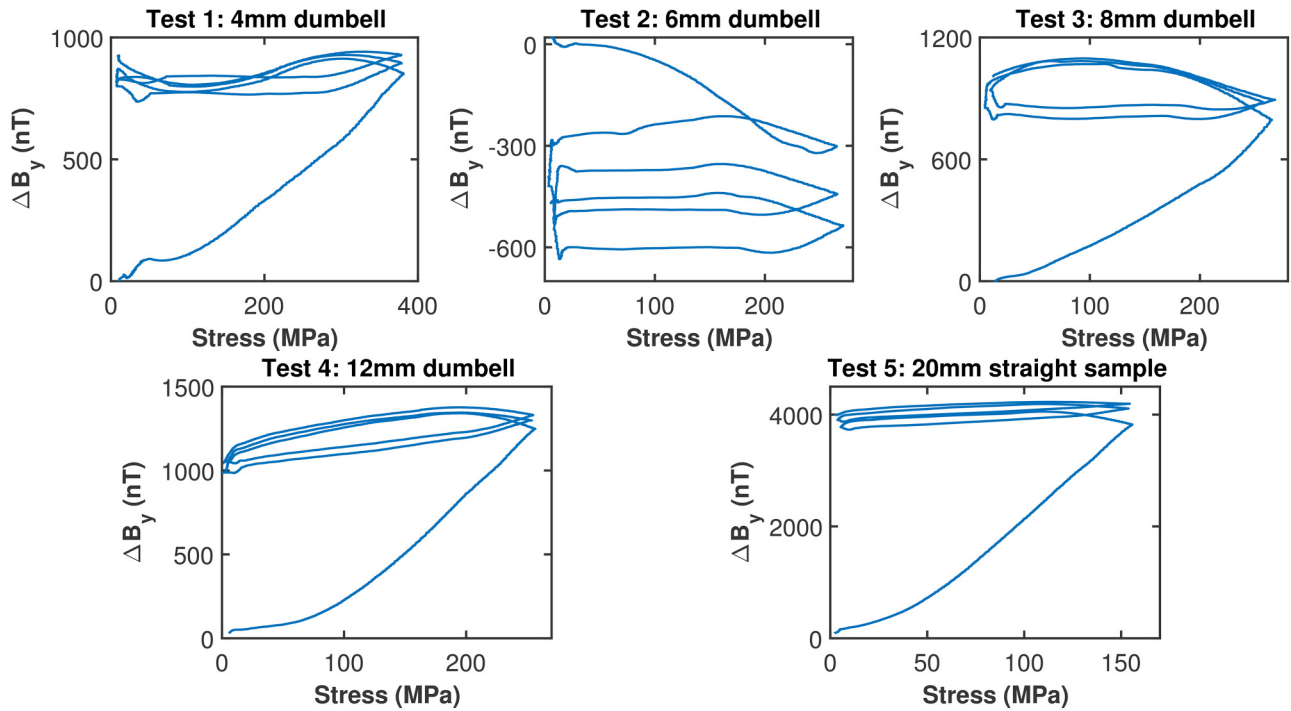


FIG. 9. Experiment 1: y-component of ΔB as a function of stress σ for all five samples, with stressing starting at the origin (0,0).

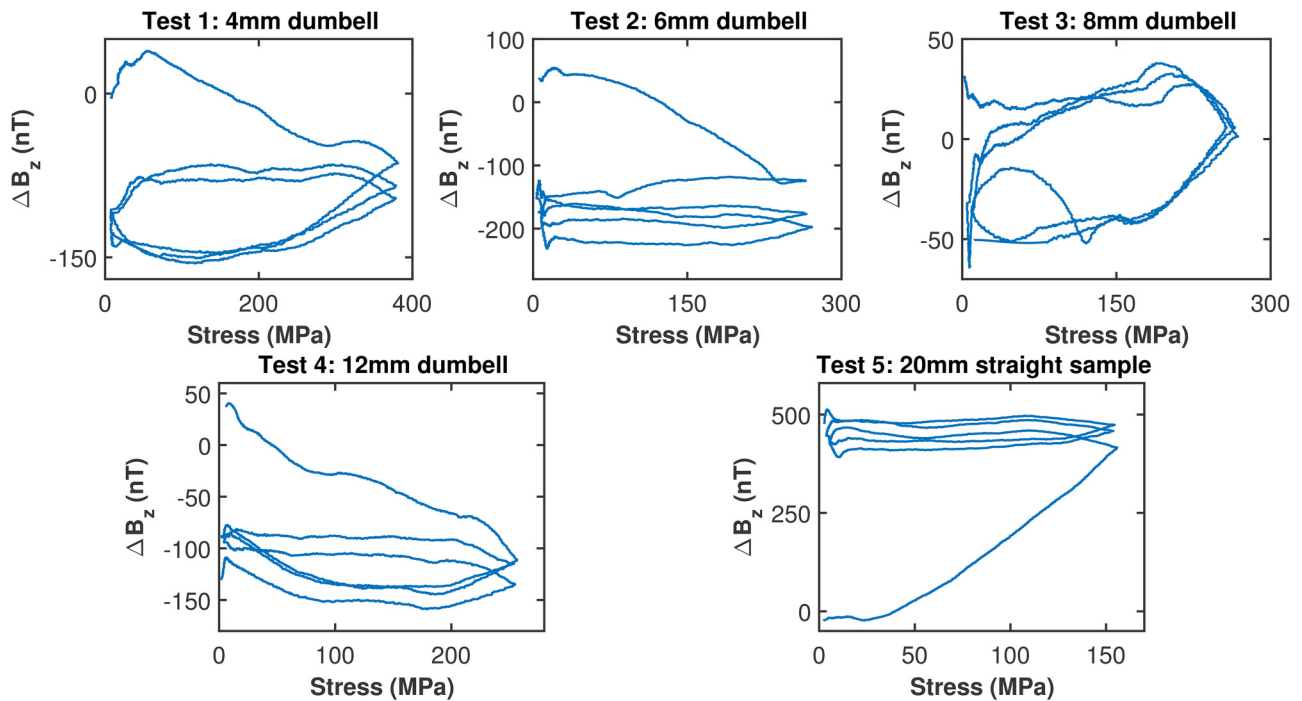


FIG. 10. Experiment 1: z-component of ΔB as a function of stress σ for all five samples, with stressing starting at the origin (0,0).

07 September 2023 08:22:43

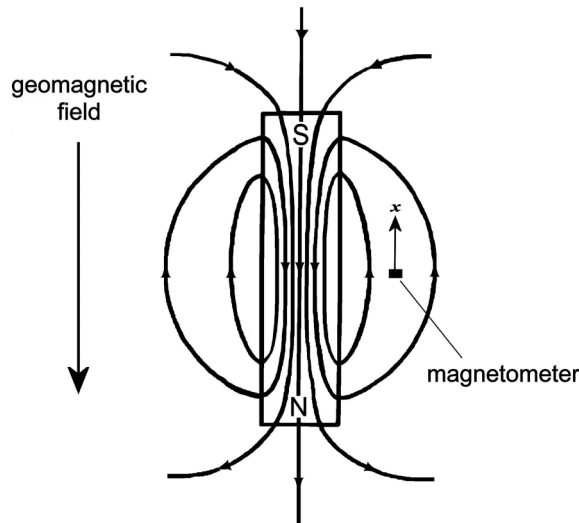


FIG. 11. If the magnetic domains within the samples are lining up in the geomagnetic field (predominantly negative x -direction) upon stressing, then we would expect a measurement at the point of the magnetometer to show changes in the positive x -direction as shown.

the level of magnetization is close to the anhysteretic level as a result of the stressing.

IV. EXPERIMENT 2: MEASURING THE MAGNETIC FIELD ON ONE SIDE OF A STEEL SAMPLE BEFORE AND AFTER STRESSING

A. Experiment 2: Motivation

In the three-cycle experiments, B -field readings were taken at one point only while the steel bar was being subjected to stress by a machine which itself had an effect on the magnetic field around the sample. In order to get a more complete picture of the magnetic field around a steel bar in both unstressed and post-stress conditions, and to obtain this picture under conditions that were less likely to have significant background interference, it was decided to take magnetometer measurements in a raster type

TABLE VI. Experiment 1: table showing the dot products (correlations) of the five pairs of unit vectors for the five tests: for each pair one vector is the unit vector giving the direction of the total background field in the forward direction, ($B_{local} + B_{machine1}$), and the other unit vector gives the direction of ΔB at the end of the stress cycling.

Test No.	Sample width (mm)	Maximum stress (MPa)	Dot product
1	4.0	407.09	-0.985
2	6.0	281.32	-0.906
3	8.0	280.73	-0.888
4	12.0	306.72	-0.842
5	20.0	167.15	-0.870

TABLE VII. Experiment 2: dimensions of the two steel bars used for the magnetic field mapping experiment.

Sample shape	Dumbell	Straight
Sample width (mm)	20.15 ± 0.01	19.99 ± 0.01
Width of middle section (mm)	4.02 ± 0.01	...
Thickness (mm)	3.00 ± 0.01	3.00 ± 0.01
Length (mm)	200 ± 1	211 ± 1
Length of middle section (mm)	80 ± 1	...
Approx. maximum force (kN)	4	10
Approx maximum stress (MPa)	326	165

fashion on one side of a bar, first in an unstressed condition, and second immediately after being stressed on the tensile test machine.

B. Experiment 2: Experimental setup and procedure

This experiment was carried out on two previously untested steel bars made from C45 carbon steel: one dumbbell-shaped bar and one straight bar, and the dimensions of both bars are given in Table VII. Prior to the experiment, the samples were prepared by a degaussing technique, to reduce their level of magnetization.

This experiment was set up such that the magnetometer was positioned under a wooden board on which was a marked grid of dimensions 28 cm by 28 cm, as shown in Figs. 12 and 13. The magnetometer and grid remained static and the steel bar was moved around the grid in the x - y plane, measurements being taken at points 2cm apart in the x - and y - directions. To obtain three different sets of readings in the z -direction the board was placed at three different levels in relation to the magnetometer, these being 43, 126, and 171 mm from the center of sensing elements with an uncertainty of 1 mm, and thus giving readings at three points on the negative z axis. The constraints of the dimensions of the sample in relation to those of the board allowed for 14 readings to

07 September 2023 08:22:43

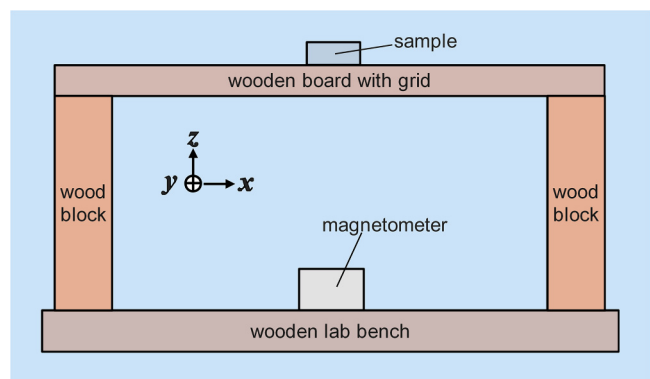


FIG. 12. Experiment 2: schematic diagram showing the experimental setup, to measure the magnetic field around a steel bar in both stressed and unstressed conditions. The flux gate magnetometer is fixed in position beneath the wooden board on which is fixed a grid. The height of the board above the bench is altered using different sized wooden blocks.

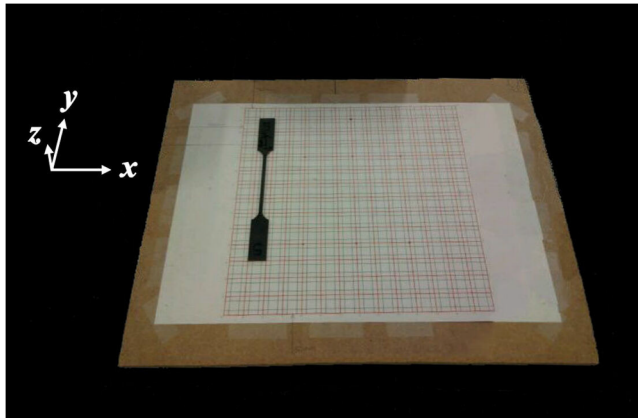


FIG. 13. Experiment 2: view of the experimental setup showing the grid upon which the steel bars were positioned for measurements of their magnetic field. The dumbbell shaped steel bar is shown placed on the grid.

be taken along the x axis and 5 readings to be taken along the y axis, for each of the three levels.

Because of constant fluctuations in the readings of the magnetic field which can be as great as 50 nT, a single magnetometer reading was taken to be the mean of 100 readings taken at 100 ms intervals. To eliminate the effect of the background B -field, a background reading was taken prior to the raster measurements at each of the three board heights which was then subtracted from the readings taken with the bar present.

For each sample, a first set of B -field readings was taken in the unstressed condition, after which the sample was stressed up to the maximum force, as indicated in Table VII, within its plastic limit, and then a second set of identically positioned readings were taken.

C. Experiment 2: Results

The measurements were plotted in Matlab as a three-dimensional vector plot with the origin of each vector at the position where the center of sensing elements of the magnetometer were in relation to the bar. Plots were made for the two samples in both their unstressed and stressed conditions with the background readings subtracted.

Looking first at the results for the straight bar: in the unstressed condition, it is evident from Figs. 14 (blue lines) and 15 (blue lines) that the sample has a B -field around it similar to that of a bar magnet with fieldlines traveling externally to the sample from the north to the south pole. This pattern is found for the field lines close to the bar, and for those further away from it. Looking at the sample after it has undergone stress (red lines), we get a similar pattern of north to south fieldlines, but in this condition, for each of the three planes, the vectors are now pointing more sharply away from the sample. It is also interesting to note that in the post-stress condition the mean magnitudes of the vectors, as given in Table VIII, are between 30% and 60% of what they were previously.

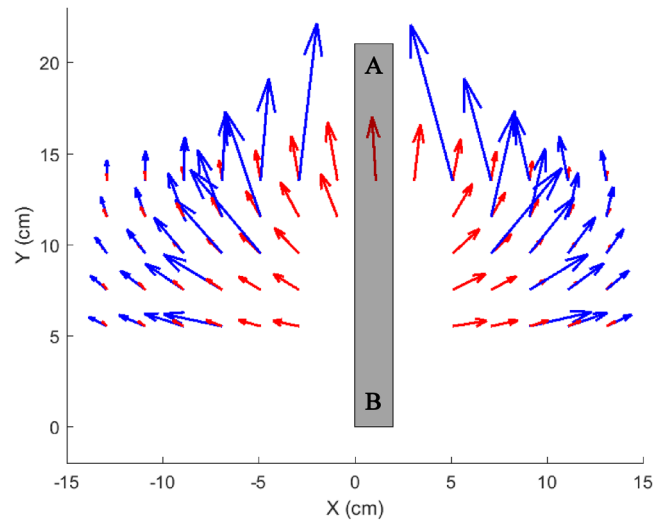


FIG. 14. Experiment 2: the B -field around the straight bar, with unstressed conditions shown in blue, and stressed conditions shown in red. For clarity the near vectors only are shown.

Looking at the dumbbell shaped bar: Figs. 16 (blue lines) and 17 (blue lines) indicate some ambiguity as to whether the field lines resemble those of a bar magnet. This could be due to the geometry of the sample which may create an effect similar to the two thicker ends acting like individual bar magnets. What is notable about the case of the dumbbell shaped bar however, is that with the stressed condition (red lines) the B -field lines now turn more sharply in toward the sample, though with some turning away at the points

07 September 2023 08:22:43

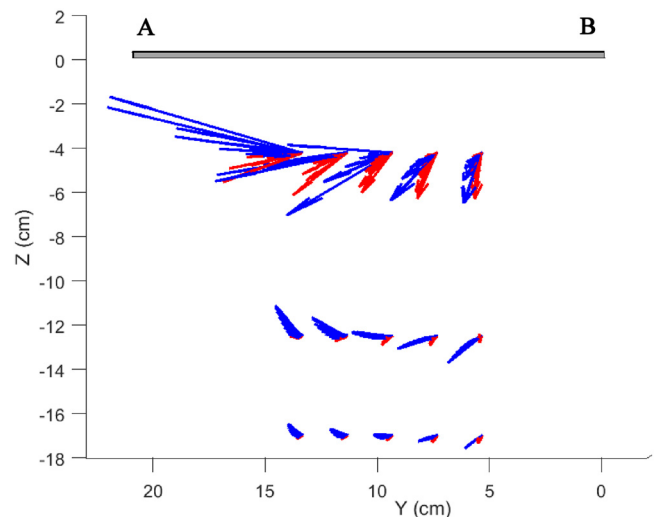


FIG. 15. Experiment 2: straight sample viewed from the side. Unstressed conditions in blue, stressed conditions in red.

TABLE VIII. Experiment 2: mean magnitudes of \mathbf{B} -field vectors for the two steel samples in stressed and unstressed conditions, at the three different levels at which the grid was placed.

z (mm)	Straight bar		Dumbbell	
	Unstressed (nT)	Stressed (nT)	Unstressed (nT)	Stressed (nT)
$-(43 \pm 1)$ "Near"	6762 ± 901	3943 ± 383	5642 ± 715	5336 ± 581
$-(126 \pm 1)$ "Mid"	4209 ± 158	1170 ± 49	1168 ± 42	1385 ± 54
$-(171 \pm 1)$ "Far"	2176 ± 56	824 ± 22	660 ± 16	1132 ± 55

that are nearer to the thin, middle part of the sample. In the near condition, the mean value of the magnitude of the vectors is reduced to about 95% of their value in the unstressed condition, but for the mid and far conditions, these values are 119% and 172%, respectively, representing an increase in vector magnitude.

D. Experiment 2: Discussion

In asking whether the results of experiment 2 confirm what was found in experiment 1, namely, that the magnetic domains of the sample appear to be lining up in the geomagnetic field, the results of experiment 2 do suggest that the polarity of each sample was starting to shift in the direction of the geomagnetic field. For the straight bar, this was a shift in the opposite direction to its existing polarity, and for the dumbbell this meant a stronger alignment along its existing polarity. However, this is a possibility rather than a certainty as the orientation of the \mathbf{B} -field due to the sample was not taken into consideration when positioning it in the local field for stressing. Hence, a useful modification to experiment 2 that could be utilized in future, similar experiments is that as the \mathbf{B} -field mapping of the sample in the unstressed state reveals the

polarity of the sample, this then needs to be taken into account when placing the sample in the geomagnetic field for stressing. This situation then presents two choices: positioning the north pole of the sample in the lower or upper position, such that the \mathbf{B} -field within the sample runs either parallel or antiparallel to the geomagnetic field. If the north pole is in the lower position and hence the orientation of the \mathbf{B} -field within the sample is parallel to the geomagnetic field, we would expect the stressing to cause the polarity of the sample to increase, or in other words, the strength of the magnet to increase, as the orientations of the domains become more lined up than they were previously. However, if the north pole of the sample is in the upper position and the \mathbf{B} -field within the magnet runs antiparallel to the geomagnetic field, we might expect the stressing to cause the orientation of the domains to start to turn in the orientation of the geomagnetic field, causing the polarity of the sample to move toward a flip.

It is possible that what happened in the current experiment is that, under stressing, the \mathbf{B} -field in the straight bar was antiparallel to the geomagnetic field, causing the overall magnetic moment of the sample to decrease. This is indicated by the \mathbf{B} -field vectors pointing more away from the sample and reducing in magnitude.

07 September 2023 08:22:43

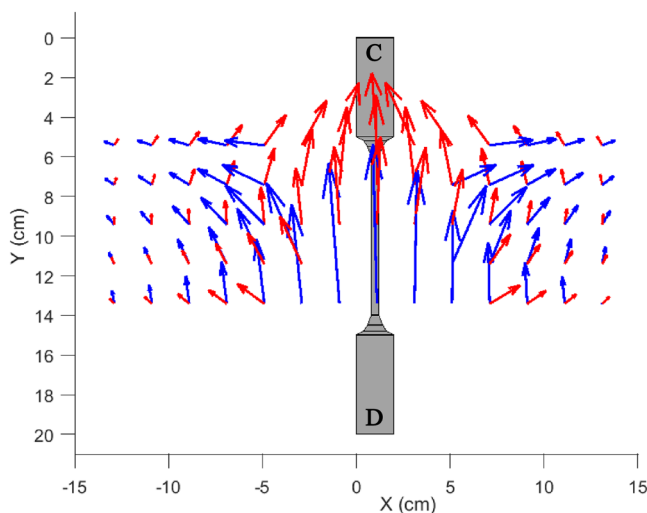


FIG. 16. Experiment 2: The \mathbf{B} -field around the dumbbell shaped bar, with unstressed conditions shown in blue, and stressed conditions shown in red. For clarity the near vectors only are shown.

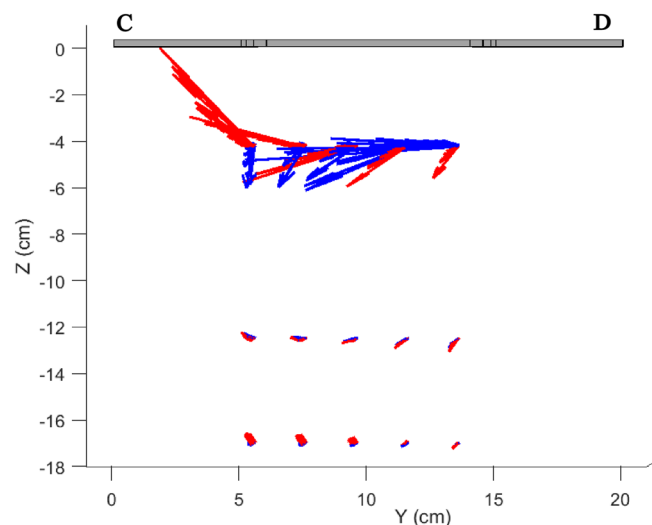


FIG. 17. Experiment 2: Dumbbell shaped sample viewed from the side. Unstressed conditions in blue, stressed conditions in red.

Conversely, for the dumbbell shaped bar, under stressing, the **B**-field in the bar may have been parallel to the geomagnetic field, causing an increase in its overall magnetic moment. This is indicated by some of the **B**-field lines moving more sharply in toward the sample and the **B**-field vectors further away from the sample increasing in magnitude. Some of the ambiguities here may be caused by the geometry of the sample, and it may be clearer to conduct this experiment with straight bars in the future.

It would also be useful to conduct this experiment with a greater number of data points in order to get a clearer picture of the **B**-field around the sample before and after stressing.

V. OVERALL DISCUSSION AND FUTURE WORK

Despite the apparent difficulty in solving the Jiles–Atherton equation for higher levels of stress, this study has shown in two different types of experiment that stressing a sample of C45 carbon steel alters the **B**-field around it, allowing us to infer that the bulk magnetization of the sample has altered as a result of the stress. These results support the hypothesis of Jiles and Atherton,⁶ and Jiles,⁸ that the underlying process of the Villari effect is that stress unpins the magnetic domains allowing them to reposition. Additionally, the results of these experiments suggest that the loosened magnetic domains orient themselves in line with the local **B**-field, which is predominantly the geomagnetic field. It is to be expected that a magnetic moment, when free to rotate, will line up in its local magnetic field. Additionally, it is worth noting that the inverse of the Villari effect, the Joule effect, is thought to be due to the magnetic domains of the sample aligning themselves in the direction of the applied magnetic field, and, by doing so, changing the shape of the sample. The fact that the loosened magnetic domains of stressed steel line up in the local magnetic field has relevance for the inverse problem of determining stress from an observed magnetic field, as posed in Staples *et al.*⁴

The experimental results reported here are closely similar to those of Craik and Wood¹² and of Birss, Faunce, and Isaac,¹³ finding that on application of uniaxial stress, a carbon steel sample will show a steady increase in magnetization attributable to the stress and that this change in magnetization will mostly remain when the sample is relaxed.

The original Jiles–Atherton model of magnetic hysteresis was suitable only for isotropic magnetic materials, but the Ramesh extension [Ramesh *et al.*;¹⁷ Szweczyk¹⁸], adapted the model to be used with anisotropic magnetic materials. Polycrystalline materials, such as the carbon steel of the experimental samples, have large numbers of magnetic domains pointing in different directions, such that the material behaves very much like an isotropic single crystal with an anisotropy energy that could be considered to be zero. However, because the application of mechanical stress causes anisotropy, and anisotropy is more apparent at low applied magnetic fields, such as the geomagnetic field, the Ramesh extension could be considered for future work of this type.

However, considering the Jiles–Atherton model of magnetic hysteresis and magnetostriction in relation to NDE, it might not be possible, even in principle, to use the Jiles–Atherton equation [Eq. (1)] to directly determine the level of stress in a sample from the measured **B**-field around it. This is because, by the law of

approach, determining which way the magnetization of a sample will change when subject to stress depends upon knowing its current magnetization state in relation to the anhysteretic level of magnetization. This would be difficult to determine in the types of structures being tested. Jiles⁸ points out that magnetization has been observed to increase or decrease under exposure to the same stress under the same external applied field. This shows that the Villari effect depends crucially on the magnetic history of the specimen in terms of its displacement from the anhysteretic due to previous magnetic field exposure and stress. In experiment 1 for the successive cycles of stress and relaxation, it was found that although the initial stress cycle caused a clear and lasting change in the magnetization of the sample, the subsequent two cycles caused a more marginal change in the same direction. This is most likely due to the limit for unpinning of the domains being reached, and an indication that the level of magnetization is close to the anhysteretic level. This suggests that using the stress–magnetization relationship for NDE works well if the material is in its first stress cycle, but after this it is difficult to know where the readings are situated on a stress curve, such as that shown in Fig. 5. However, the Jiles–Atherton model, and work related to it tells us that, given a sharp change in the **B**-field close to a sample, it would be a reasonable assumption that there could be a stress concentration zone in that region that would be worth investigating. The current work suggests that it might also be expected that the stressing of steel structures will cause a shift in the **B**-field of the steel in the direction of the geomagnetic field.

Following on from these results, a possible method of NDE of large steel structures, such as bridges or buildings, may be to place magnetometers at regular locations over the structure, and these could send regular measurements back to a central data logger and computer. The indication of formation of a stress concentration zone will be if there is a sudden change in the magnetization over one particular area. By the Jiles–Atherton theory, the change in magnetization could be either up or down, as the formation of a stress concentration zone would be expected to force the magnetization toward the anhysteretic value, and the position of the anhysteretic in relation to the current magnetization would depend on the history of the sample. However, in the light of this study, it might also be expected that stress would cause a shift in magnetization of the structure in line with the geomagnetic field, causing a shift in the **B**-field in the opposite direction external to the structure in a similar manner to that shown in Fig. 11. However, any technique involving the regular positioning of magnetometers would be challenging to apply to extended steel structures such as pipelines, due to the very long distances involved, and for pipelines, in particular, large stand off magnetometry using a moving array of magnetometers seems to be the more practical and promising option for detecting stress concentration zones.⁵

Given that the history and polarity of the sample has an effect on the surrounding **B**-field and its response to stress, it would be advantageous to combine the Villari effect technique of NDE with other NDE techniques, such as use of Barkhausen effect sensors,¹⁹ magneto-acoustic emission sensors,¹⁹ or the magnetoelastic (magnetically induced velocity change) method.¹⁹

The observation, that stressing carbon steel loosens the magnetic domains which then align themselves in the local **B**-field,

thus, in turn, altering the B-field around the steel object, provides an improved understanding of how the magnetic field around a steel object changes as a result of stress, which can be taken into account in the NDE of steel structures.

ACKNOWLEDGMENTS

The work in this paper is possible due to funding by Speir Hunter Ltd.

AUTHOR DECLARATIONS

Conflict of Interest

The authors have no conflicts of interest in relation to this work.

Author Contributions

C. A. Ives: Conceptualization (equal); Data curation (equal); Formal analysis (lead); Investigation (equal); Methodology (lead); Project administration (equal); Validation (equal); Visualization (lead); Writing – original draft (lead); Writing – review & editing (lead). **S. G. H. Staples:** Conceptualization (equal); Data curation (equal); Formal analysis (supporting); Funding acquisition (supporting); Investigation (equal); Methodology (equal); Project administration (equal); Supervision (equal); Visualization (supporting); Writing – review & editing (supporting). **C. K. Vo:** Project administration (equal); Writing – review & editing (supporting). **D. M. J. Cowell:** Project administration (equal); Writing – review & editing (supporting). **S. Freear:** Project administration (equal); Supervision (supporting); Writing – review & editing (equal). **B. T. H. Varcoe:** Conceptualization (equal); Formal analysis (equal); Funding acquisition (equal); Investigation (equal); Methodology (equal); Project administration (equal); Supervision (equal); Writing – review & editing (equal).

DATA AVAILABILITY

The data that support the findings of this study are available from the corresponding author upon reasonable request.

REFERENCES

- ¹E. Villari, “Change of magnetization by tension and by electric current,” *Ann. Phys.* **126**, 87–122 (1865).
- ²J. P. Joule, “On the effects of magnetism upon the dimensions of iron and steel bars,” *Lond. Edinb. Dublin Philos. Mag. J. Sci.* **30**, 76–87 (1847).
- ³E. Lee, “Magnetostriction and magnetomechanical effects,” *Rep. Prog. Phys.* **18**, 184–229 (1955).
- ⁴S. G. H. Staples, C. Vo, D. M. J. Cowell, S. Freear, C. Ives, and B. T. H. Varcoe, “Solving the inverse problem of magnetisation–stress resolution,” *J. Appl. Phys.* **113**, 133905 (2013).
- ⁵S. Staples, B. Varcoe, C. Vo, D. Cowell, C. Cookson, and S. Freear, “Bar magnet model for large stand off magnetometry” (unpublished).
- ⁶D. C. Jiles and D. L. Atherton, “Theory of ferromagnetic hysteresis,” *J. Magn. Magn. Mater.* **61**, 48–60 (1986).
- ⁷D. Jiles and D. Atherton, “Theory of the magnetization process in ferromagnets and its application to the magnetomechanical effect,” *J. Phys. D: Appl. Phys.* **17**, 1265–1281 (1984).
- ⁸D. Jiles, “Theory of the magnetomechanical effect,” *J. Phys. D: Appl. Phys.* **28**, 1537–1546 (1995).
- ⁹G. Wiedemann, *Philos. Mag.* **52**, 31 (1886).
- ¹⁰A. Globus and P. Duplex, “Initial susceptibility of ferrimagnetic materials and topography of domain walls,” *Phys. Status Solidi* **31**, 765–774 (1969).
- ¹¹A. Globus and P. Duplex, “Size of Bloch wall and parameters of the magnetic susceptibility in ferrimagnetic spinels and garnets,” *Phys. Status Solidi A Appl. Mater. Sci.* **3**, 53–61 (1970).
- ¹²D. Craik and M. Wood, “Magnetization changes induced by stress in a constant applied field,” *J. Phys. D: Appl. Phys.* **4**, 1009–1031 (1971).
- ¹³R. Birss, C. Faunce, and E. Isaac, “Magnetomechanical effects in iron and iron-carbon alloys,” *J. Phys. D: Appl. Phys.* **4**, 1040–1051 (1975).
- ¹⁴L. Li and D. Jiles, “Modified law of approach for the magnetomechanical model: Application of the Rayleigh law to stress,” *IEEE Trans. Magn.* **39**, 3037–3039 (2003).
- ¹⁵See <https://saemobilus.sae.org/standards/> for “SAE (Society of Automotive Engineers) International” (last accessed April 26, 2022).
- ¹⁶See http://geomag.nrcan.gc.ca/calc/mfc/r-en.php?date=2012-02-07&latitude=53.8008&latitude_direction=1&longitude=1.5491&longitude_direction=-1 for “Natural Resources Canada” (last accessed May 15, 2016).
- ¹⁷A. Ramesh, D. Jiles, and J. Roderick, “A model of anisotropic anhysteretic magnetization,” *IEEE Trans. Magn.* **32**, 4234–4236 (1996).
- ¹⁸R. Szewczyk, “Validation of the anhysteretic magnetization model for soft magnetic materials with perpendicular anisotropy,” *Materials* **7**, 5109–5116 (2014).
- ¹⁹D. Jiles, *Introduction to Magnetism and Magnetic Materials* (Taylor & Francis, 1998).

07 September 2023 08:22:43